A cerebellar window for intravital imaging of normal and disease states in mice

Vasileios Askoxylakis[1,6,7], **Mark Badeaux**[1,2,7], **Sylvie Roberge**[1], **Ana Batista**[1,3], **Ned Kirkpatrick**[1,4], **Matija Snuderl**[1,5], **Zohreh Amoozgar**[1], **Giorgio Seano**[1], **Gino B Ferraro**[1], **Sampurna Chatterjee**[1], **Lei Xu**[1], **Dai Fukumura**[1], **Dan G Duda**[1], and **Rakesh K Jain**[1]

[1]Edwin L. Steele Laboratories, Department of Radiation Oncology, Massachusetts General Hospital and Harvard Medical School, Boston, Massachusetts, USA

[2]Aeglea Biotherapeutics, Austin, Texas, USA

[3]Cell Press, Cambridge, Massachusetts, USA

[4]Novartis Cambridge, Massachusetts, USA

[5]Department of Pathology, New York University Langone Medical Center and Medical School, New York, New York, USA

Abstract

The cerebellum is a prominent part of the vertebrate hindbrain that is critically involved in the regulation of important body functions such as movement coordination, maintenance of balance and posture, and motor control. Here, we describe a cerebellar window that provides access to the mouse cerebellum for intravital imaging, thereby allowing for a detailed characterization of the dynamic processes in this region of the brain. First, the skull overlying the cerebellum is removed, and then the window is applied to the region of interest. Windows may be exchanged depending on the desired imaging modality. This technique has a variety of applications. In the setting of medulloblastoma, spontaneous or orthotopically implanted lesions can be imaged, and tumor morphology and size can be monitored using ultrasonography. Multiphoton laser-scanning microscopy (MPLSM) or optical-frequency-domain imaging (OFDI) can be applied for *in vivo* visualization and analysis of cellular and vascular structures in a variety of disease states, including malignancies and ataxia telangiectasia. This protocol describes a novel and rapid method for cerebellar window construction that can be set up in under an hour.

Publisher's note: Springer Nature remains neutral with regard to jurisdictional claims in published maps and institutional affiliations.

INTRODUCTION

The cerebellum is a critical region of the vertebrate hindbrain that is responsible for integrating sensory-input signals into coordinated muscular movement. It may be adversely affected in a number of pathological conditions, including genetic neurodegenerative disease, such as ataxia telangiectasia; inflammatory states, such as cerebellitis; and neoplasias, including medulloblastoma. Intravital imaging is critical to gaining a better understanding of these conditions.

Pediatric medulloblastoma, of particular interest to our group, is the most common malignant brain tumor in children and represents a complex clinical problem. Standard-of-care treatments, including radiation, surgical resection, and chemotherapy, vary greatly in efficacy, but cause substantial morbidity and quality-of-life reduction in patients. Preclinical models are key to developing and testing novel, more efficacious, and safer therapies. *In vivo* imaging is necessary, in order to study tumor initiation, growth, morphology, and response to therapy.

The intact mouse skull is sufficiently thick to prevent direct imaging of the brain with high resolution. One technique used to circumvent this obstacle is to thin the cranial bone to a thickness (~20 μm) that allows optical imaging[1–3], albeit with a slight loss of resolution. To optimize imaging fidelity, we and others developed chronic cranial windows, a technique in which a circular area of the cranial bone is replaced with a glass coverslip through which the cortex can be imaged in live[4–6], and even awake[7], mice. In this protocol, we describe how to insert a cerebellar window into mice. We developed this method to facilitate our study of preclinical models of medulloblastoma[8], although the window has potential applications beyond the study of brain tumors, as discussed below. This window was used for the preclinical investigation of critical tumor–stroma interactions across medulloblastoma subtypes[8], and use of the cerebellar window greatly aided in studies that identified the role of the PlGF/Nrp1 pathway in pediatric medulloblastoma[8].

Applications of the protocol

In the context of cancer, cranial-window techniques may be used to longitudinally study brain tumors in the cortical area, including glioblastoma and breast cancer brain metastases[9–14]. In particular, cranial windows enable intravital MPLSM, which is useful for observing the dynamic growth and migration of fluorescently labeled tumor cells. When used in the setting of stromal architecture also tagged with a fluorochrome, or when imaging stromal components that exhibit second-harmonic generation, it is possible to study the interaction of the tumor and its stromal milieu at subcellular resolution. Imaging of drug delivery by MPLSM can also be facilitated by studying compounds that are inherently fluorescent or by using antibody conjugates that bear fluorescent tags[15]. To complement MPLSM, OFDI[11,16] can provide a high-resolution map of the vasculature in normal, premalignant, or tumorous tissue. In addition, high-frequency ultrasonography may be used in order to accurately measure the tumor volume, especially at depths at which the other imaging modalities are unable to function. Importantly, this technique can be coupled to the measurement of *Gaussia* luciferase (Gluc) levels in the blood of mice bearing stably

transduced tumors[17,18], thereby allowing for the noninvasive measurement of tumor volume in situations in which direct imaging is impractical or unavailable.

Although tumors in the murine cortical region have been extensively imaged via intravital methodologies, tumors arising in the cerebellum, such as medulloblastoma, have received comparatively less attention. Previous studies used approaches such as MRI to measure medulloblastoma volume[19,20], but this technique is costly and time-consuming, making arbitrary or serial measurements infeasible. To study these tumors, it is imperative to adapt and suit the imaging modalities to the unique topology of the cerebellum. Here, we present an optimized version of the cranial window, which we term a 'cerebellar window', and which can be used for optical access to the mouse cerebellum. In this technique, we confine the region of skull replacement to the area overlaying the cerebellum. Furthermore, the choice of the imaging modality can be optimized through the use of a glass (for MPLSM or OFDI) or polyethylene (for ultrasonography) cover-slip. Importantly, we demonstrate that constitutively expressed, tumor-cell-specific Gluc can be measured in the blood and used as a surrogate measure of tumor volume, once ultrasonography has been used to standardize the tumor volume as a function of blood Gluc levels. Moreover, the cerebellar window allows for the rapid detection and monitoring of spontaneous medulloblastoma in genetically engineered mouse models (GEMMs). In addition, we show that salient features of the tumor pathophysiology, including tumor vessel morphology and drug delivery, can be accurately described during a clinically relevant medulloblastoma treatment protocol.

Alternative methods

Studying the onset and progression of pediatric medulloblastoma in mouse models, especially GEMMs, is very challenging, mostly owing to the heterogeneity in latency, location, and growth pattern, as well as the lack of clinical symptoms at early stages of the disease. Owing to excellent tissue contrast, MRI represents the state-of-the-art clinical-imaging modality for medulloblastoma, other brain tumors, and indeed for most cerebellar disease states. However, the use of conventional MRI, which does not require the establishment of a window, in preclinical models is very challenging, and, in most cases, it is limited to determining tumor progression at later, advanced stages of the disease[21,22]. Recently, more advanced MRI protocols for high-resolution imaging of medulloblastoma tumors at early stages in mice have been developed and optimized[20]. However, these approaches have some limitations. High-resolution imaging is very time-consuming, whereas rapid, high-throughput imaging can be performed at the expense of resolution[20]. Despite recent advances, the resolution limit of MRI-based approaches is ~50 μm.

Advantages and limitations

Performing qualitative and quantitative analysis of dynamic biological events requires high-resolution imaging technologies. The development of such technologies, including MPLSM and OFDI[11], has facilitated the mechanistic exploration of pathophysiological processes in tumors. However, these technologies require, in most cases, direct optical access to the tumor through a window[23,24]. The cerebellar window presented here provides optical access to the mouse cerebellum, allowing the intravital imaging of medulloblastomas.

Experimental design

Here, we describe a protocol for implementing a window-based approach for imaging the murine cerebellum (Fig. 1). The cerebellar window provides optical access to the mouse cerebellum and can be used for multimodal visualization of structural, morphological, and functional characteristics of both normal tissue and malignancies in this environment. Moreover, the development and growth of both implanted and spontaneous cerebellar tumors can be effectively monitored, vessel features can be measured, and drug delivery can be determined. In addition, there are a number of critical steps as noted in the detailed protocol that require preparation before beginning this study. For instance, it is useful—at the study's inception—to map the imaging that is necessary throughout, as this will inform the choice, timing, and placement of the respective coverslips that are specific to each imaging modality. In addition, it is important that all surgical tools be sterilized (we autoclave all surgical tools routinely) before beginning the procedure.

Below we present some technical considerations.

Surgery and follow-up care—The surgical procedure used to implant the window, the follow-up care, and the subsequent imaging each present a number of technical considerations that are important determinants of successful long-term intravital imaging. The portion of the skull overlying the cerebellum can be removed and the coverslip can be placed in a single surgical event. However, it is recommended to wait for at least 1 week for potential inflammation to subside before imaging. After this period, tumor cells can be implanted (when desired) during a second surgery (Supplementary Fig. 1). This second surgery is not required in imaging GEMMs. Although a second surgery under anesthesia presents a health risk to the mouse, it is important that implantation does not occur in the setting of local inflammation, as the tumor kinetics becomes more variable and the model less faithfully represents the clinical reality. Despite previous reports of reactive gliosis in the cortex after implantation of a cranial window[6], analysis of the cerebellum 2 d and 10 d after cerebellar window implantation did not reveal clear glial activation as compared with the control tissue (Supplementary Fig. 2).

The quality of each surgery and the health of the mouse are also key determinants of imaging quality, as hemorrhage or tissue damage can obscure key features of the brain and tumor architecture. The dura mater, if left intact during the initial surgical procedure, can thicken over time, leading to loss of optical quality[6]. Once the cerebellar window is established, the coverslip can be changed to accommodate multiple imaging modalities. However, each change requires surgical intervention and carries the risks associated with any invasive procedure that involves anesthesia. Therefore, although the coverslip can be changed, we do so sparingly. Once a coverslip is affixed to the cranium, it is possible to image longitudinally for a period of up to about five months, after which time, bone regrowth can limit the resolution and imaging quality.

Imaging method selection—Immunohistochemical (IHC) analysis is the most widely used method to investigate tumor biology by imaging. However, these static images do not permit the examination of dynamic changes occurring during the natural history of the

disease. Intravital microscopy allows longitudinal and quantifiable imaging of the orthotopic environment. The use of transparent windows, as described in our protocol, has substantially transformed our view of tumors. However, the selection of the most appropriate imaging method is essential.

The quantification of microvascular perfusion is a prime example of the measurement of the same biological feature using different methods of imaging. Microbubble injection combined with ultrasonography allows the quantification of perfusion of the whole volume of the tumor, with low resolution but with a wide field of view[25]. OFDI permits fast and accurate imaging, and quantification of perfused vessels and their geometry within the 1-mm most superficial layer of tissue of the whole transparent window area with no need for tracers, but it is unable to visualize nonperfused vessels. MPLSM may be more versatile, but is time-consuming and limited in imaging depth; it can be combined with injection of labeled red blood cells to quantify blood-flow velocity[26] with endothelial cell reporter mice and injection of blood-flow tracers to visualize perfused and nonperfused vessels, or can be combined with other fluorescently tagged cells of the tumor microenvironment to visualize how these cells modify vascular perfusion locally[27,28]. IHC of lectin-perfused tissues can be used to confirm the results from intravital micrscopy (IVM) in terms of the percentage of perfused vessels[29]. Methods that do not require a window model, such as MRI or micro-CT, can also provide a measurement of blood flow and/or perfusion[30]; however, they are limited in spatial resolution, and thus cannot resolve the tumor microvasculature. The use of *ex vivo* micro-CT imaging of vascular casts can provide a 3D high-resolution image of the microvasculature[31], but, similar to IHC, it represents a single, static time point.

Sample size calculation—To obtain a sufficient number of mice with cerebellar windows, the survival rate post surgery should be considered. Even when considering the need for multiple surgeries in order to introduce tumor cells into the cerebellum, the overall survival rate after multiple surgical interventions for most mouse strains lies between 70 and 90%. This number varies with the experience and skill level of the scientist performing the surgeries.

Cost and time—The cerebellar window approach described in this protocol costs relatively little in terms of reagents. We have noted that, on occasion, mice mechanically interfere with or attempt to displace their cage mates' cerebellar windows. For this reason, we customarily house them individually after implantation of a cerebellar window. In the case of xenograft tumors, the mice must be housed for at least 10 d before implantation of tumors. This is of particular importance if any immunological studies are planned, as recovery from inflammation, as described above, is necessary before tumor-cell implantation or imaging of processes at single-cell resolution. After tumor-cell implantation, the mice should be housed for a healing period of at least 3–7 d. The time line for an experimental study routinely extends up to several weeks or months; in the setting of tumors, this number depends on many variables, including tumor latency, rate of growth, and efficacy of treatments administered, among other factors. Cost calculations for studies of mice with cerebellar windows must therefore also consider animal housing during this time period. In regard to the time and effort necessary to establish cerebellar windows, the implantation of a

cerebellar window takes about 45–60 min. However, this minimal time requires high surgical expertise; absent this, implantation may take longer.

Applications of the cerebellar window

Small-animal ultrasonography—Ultrasonographic (US) imaging represents an attractive imaging modality for the evaluation of therapeutic response in oncology. Major advantages of US imaging include an excellent temporal resolution without exposure to irradiation. The development of 3D dynamic-contrast-enhanced (3D-DCE) US imaging allows not only the accurate volumetric measurement of tumor size but also the monitoring of functional parameters, such as tumor perfusion. In this way, US imaging enables not only the noninvasive longitudinal evaluation and quantification of morphologic and anatomic changes in tumors but also the quantification of treatment effects before the morphological changes become visible[32].

US imaging is widely used for tumor imaging in preclinical models. Small-animal ultrasound imaging includes the detection of tumors and their metastases[33,34], the monitoring of tumor growth and response to therapies[13,35], as well as the characterization of the tumor vascularity[36,37]. High-resolution US imaging of the brain or the cerebellum is limited because of the high acoustic impedance of the bones of the skull. A cranial window with a polyethylene coverslip allows sound waves to pass through the brain tissue and therefore permits the high-resolution imaging of primary and secondary brain tumors. This procedure has been extensively utilized by our group for the evaluation of therapeutic drugs in preclinical models of glioblastoma and brain metastases[13,29].

The cerebellar window described in this protocol allows the high-resolution ultrasound imaging of stereotactically implanted (Fig. 2a) or spontaneous medulloblastoma tumors (Fig. 2b) in mouse models. For our studies, we use the VisualSonics Vevo2100 High-Resolution Ultrasound System. With respect to spontaneous medulloblastoma in GEMMs, ultrasound imaging is a very efficient and advantageous alternative to MRI-based imaging, primarily because of the necessity for serial imaging, as (i) the tumor onset and development of these tumors cannot be predicted, and (ii) repeated imaging and quantification of the tumor volume is necessary to obtain essential information on tumor growth kinetics. Serial ultrasound-based imaging is both time- and cost-effective: Ultrasonography through the cerebellar window, including data analysis, can be performed within 15–30 min. Moreover, using a 3D motor frame and a stereotactic system, ultrasound imaging allows the rapid 3D reconstruction of tumor volume for medulloblastoma tumors (Fig. 2c).

In addition, rapid ultrasonography-based imaging of implanted medulloblastoma models can be applied for the evaluation of indirect surrogates of tumor growth. Specifically, we have previously developed orthotopic models of medulloblastoma using human tumor cells that were engineered to express secretable Gluc in the blood[8]. Gluc expression in the tumor can be used for local detection and visualization of cerebellar tumors with bioluminescence imaging (Fig. 3a). Gluc activity in serum can additionally be used as a precise surrogate measure to monitor tumor growth, provided that there is a strong correlation between Gluc activity and real tumor volume. Concomitant measurement of the 3D tumor volume using ultrasound and Gluc activity in the serum provides important information on the correlation

between the two parameters (Fig. 3b). Furthermore, longitudinal imaging studies to test therapeutic response can be based on the fast and simple measurement of serum Gluc activity, rather than on the direct imaging of tumor burden (Fig. 3c,d).

Ultrasound-based imaging of medulloblastoma tumors through a cerebellar window is a multistep approach that includes (i) preparation of the mice for imaging, (ii) 2D and/or 3D image acquisition, and (iii) postimaging analysis of the data; each of these steps can be performed within a time frame of 5–10 min.

Multiphoton microscopy—IVM allows the achievement of two key tasks in tumor biology: the behavioral observation of cells, tissues, and/or organs within the real environment (i.e., *in vivo*), and the quantification of biological and clinically relevant phenomena. Various parameters can be quantified by IVM. These can range from parameters disclosed by very high magnification—molecular and subcellular imaging (1-μm resolution), to those revealed by imaging at the cellular level—cell tracking (10-μm resolution), and finally to those displayed by functional–anatomical imaging—tumor size, vascular architecture, blood-flow rate, vascular permeability, drug distribution, and uptake (resolution from tens to hundreds of microns)[28,38,39]. To build an IVM model, four elements are needed: an appropriate animal model with a transparent window; a molecular fluorescent probe— injected fluorophore-tagged tracers or reporter fluorescent proteins (produced by viral transduction or specific promoters in transgenic mice)—that can be imaged; a microscope with an appropriate imaging depth and equipped with an excitation source and a detection system; and image-analysis algorithms applied to extract quantitative data.

IVM has been a critical tool and has led to numerous discoveries in the field of tumor biology. Vascular functionality has been discovered to be strongly impaired in tumors[40], so objective intravital visualizations and quantifications of perfusion[27], pH, pO_2 and NO gradients[41–43], red blood cell velocity[26], permeability and pores[44], diameter and architecture[11,13,45,46], and maturation[46,47] of tumor vasculature are important tools to gain clinically relevant insights into tumor physiopathology.

IVM allows the quantification of rolling, extravasation, migration, and infiltration of macrophages, leukocytes and lymphocytes within the tumor mass, as well as the investigation of the involvement of fibroblasts during tumor progression[48–52]. Collagen fibers are important modulators of tumor stiffness and solid stress, and consequently of tumor progression and drug delivery[53,54]. Impaired drug delivery within the tumor mass is an important and clinically relevant issue. IVM allows us to visualize the regions with low drug diffusion, delivery, and/or efficiency (e.g., small molecules, antibodies, liposomes, and nanoparticles) that occur in many tumors[40,44,55]. Finally, IVM has been essential in the description of the first steps of the process of formation of distant metastases[56]. IVM enabled the discovery and visualization of the involvement of cell-to-cell interactions of specific macrophages with metastatic tumor cells during the intravasation process[57,58].

Using the cerebellar window, multiphoton laser-scanning microscopy of cerebellar tumors is enabled (Fig. 4). This allows the visualization of both tumor cells and the tumor vasculature in the microenvironment of the cerebellum, as well as (Fig. 4a–c) the quantitative analysis of

tumor characteristics (Fig. 4d,e), which is necessary to better understand the pathophysiology of medulloblastoma.

Optical frequency-domain imaging—Optical coherence tomography (OCT), an imaging method that uses the light-scattering properties of soft tissue in order to generate high-resolution maps of anatomical structures, is extremely useful in preclinical imaging studies. Importantly, it is amenable to the study of the brain when used in tandem with a cranial window, and it has been shown to be extremely useful in delineating normal cerebellum from tumor tissue in genetically engineered mouse models of medulloblastoma[59]. In our laboratory, we use a second-generation form of OCT, known as optical frequency domain imaging (OFDI)[11]. Much like other *in vivo* imaging methods that capture high-resolution images, it is important that the mouse, or at least the anatomical location of the mouse that is to be studied, is immobilized during imaging sessions. It is only slightly inferior to MPSLM in terms of resolution, and is far superior to ultrasonography or MRI in this regard. OCT can be used to image tissue at depths of up to 2 mm, as it uses longer, near-infrared wavelengths of light. Its applications include cerebellar tumor volume measurements for smaller tumors, angiography, and assessment of tissue viability[24]. One advantage of this technology is that multiple biological parameters such as those described above can be assessed quickly in one scan. The entire brain/cerebellum can be imaged in 1–20 min; however, imaging time is inversely correlated to image contrast. Postprocessing analysis then yields a detailed picture of the parameter of interest (Fig. 5a,b). It is also ideal for longitudinal studies and arbitrary repeated measurements, as OCT/OFDI does not require the addition of an exogenous label that may impair image quality over time (Fig. 5c). In our laboratory, using the cerebellar window, it is possible to toggle between cerebellar ultrasonography and MPSLM/OFDI by simply applying a different coverslip to the cranium of the mouse; this allows us to capitalize on the relative strengths of multiple imaging modalities in a single study (for a comparison of these modalities, see ref. 44).

MATERIALS

REAGENTS

- Mice: Nude, SCID or nod-SCID mice are preferred for orthotopic implantation of human medulloblastoma cell lines. Nude, SCID and nod-SCID mice are bred and maintained at the Gnotobiotic Mouse Cox 7 Core at the Massachusetts General Hospital (https://researchcores.partners.org/cox/about). GEM medulloblastoma models (obtained from the Jackson Laboratory) are used for spontaneous medulloblastoma tumors

  ! CAUTION All animal studies must be reviewed and approved by the relevant animal-care committees and must conform to all relevant institutional and national ethics regulations. All animal procedures were performed according to the guidelines of the Public Health Service Policy on Human Care of Laboratory Animals and were in accordance with a protocol approved by the Institutional Animal Care and Use Committee of Massachusetts General Hospital. ▲ **CRITICAL** For experiments on pediatric medulloblastoma, it is important to

use young mice (4–6 weeks old). Within one experiment, we recommend using only one gender of mice in order to minimize variability.

- Anesthesia: Ketamine (use at 90 mg/kg body weight) and xylazine (use at 9 mg/kg body weight). Both medications are added to sterile saline to obtain the described concentrations. Ketamine (Ketaset, 100 mg/ml; Patterson Veterinary, cat. no. 07-803-6637) and xylazine (AnaSed, 100 mg/ml, Patterson Veterinary, cat. no. 07-808-1939)

- Analgesia: Buprenorphine (Buprenex, 0.3 mg/ml; Patterson Veterinary, cat. no. 07-850-2280) is used at a concentration of 0.1 mg/kg ▲ **CRITICAL** Buprenorphine is to be injected s.c.

- Saline, sterile (to dilute ketamine and xylazine), sodium chloride, 0.9%, bacteriostatic, 30 ml (Hospira, cat. no. SKU ABB19660715Z) or similar

- Saline, 0.9%, for irrigation (Owens-Minor, cat. no. 0706-2F7123)

- Cell lines: the human pediatric medulloblastoma cell lines used in our studies are D283 and D341 (ATCC, cat. nos. HTB-185 and HTB-187)

  ! CAUTION The authenticity of any cell line should be confirmed by short tandem-repeat allelotyping or another genetics-based confirmation method before use; the cell lines should also be confirmed to be mycoplasma-free.

- Ophthalmic lubricant

EQUIPMENT

- Stereotactic frame (the authors use a custom-built model for window preparation, but David Kopf's small-animal stereotactic apparatus model no. KOPF921 or a similar model can be used for tumor cell implantation)

- Bright-field stereomicroscope (Olympus, model no. SZ61 or similar)

- Thermal pad (Shor-Line, model no. 712.0000.04 or similar)

- Bone microdrill for brain surgery (Harvard Apparatus, model no. PY272-4950 or similar)

- Coverslip, 7 mm, glass (Fisher, cat. no. 7-CIR-1-Fisher or similar) or polyethylene (Ted Pella, cat. no. 2225, custom cut in-house or similar)

- Syringe, 10-μl (Hamilton, cat. no. 7635-01 or similar)

- 2-inch PT2 needle (Hamilton, cat. no. 7635-01 or similar)

- Ophthalmic lubricant, (Paralube; Patterson Veterinary, cat. no. 07-888-2572 or similar)

- Sterile gauze, any

- BD tuberculin syringe, 1 ml, 26-gauge needle (Fisher, cat. no. 14-823-2E)

- Sterile cotton tip applicators (Owens and Minor, cat. no. WOD1002 or similar)

- Sterile Gelfoam, hemostatic size 100 (McKesson, cat. no. 189842)

- Sponges, 3-inch × 3-inch (Cardinal Health, cat. no. 3307394)

- Krazy Glue, all-purpose, one-drop applicator or a similar histocompatible cyanoacrylate glue

- Extra-fine acrylic powder, dental or nail grade

- Marking pen, any

- Straight iris scissors (Bonn, cat. no. RS-5840 or similar)

- Vannas spring scissors (Bonn, cat. no. RS-5611)

- Straight forceps (Bonn, cat. no. RS-8140)

- Dumont forceps no. 3 and no. 5 (Bonn, cat. nos. RS-5042 and RS-5045, respectively)

- Cotton swabs

REAGENT SETUP

Anesthesia mix—Prepare an anesthesia mix by diluting ketamine and xylazine in sterile saline at a ratio of 10:1. The ketamine/xylazine mixture can be made in advance and stored at room temperature (25 °C) for several weeks.

PROCEDURE

Surgery ● TIMING 45 min

1| Administer buprenorphine at 0.1 mg/kg body weight s.c. 15 min before surgery. Anesthetize the mouse with 90 mg/9 mg per kg body weight of a ketamine/xylazine mixture. Ensure that the mouse is sufficiently anesthetized by testing its pedal reflex and monitoring its respiration.

! CAUTION All experiments with mice should be performed while following institutional and national guidelines.

2| Apply an ophthalmic lubricant to the eyes.

3| Remove a 10-mm circular disk of skin and connective tissue from the skull in the posterior part of the head. Expose and clean the periosteum to the temporal crests with a sterile cotton swab.

4| Place the mouse in the stereotactic frame and stabilize the head under the bright-field stereomicroscope.

▲ CRITICAL STEP Ensure that the position of the mouse is secure.

5| Wash the scalp with sterile saline.

▲ CRITICAL STEP Do not apply ethanol to open wounds or an exposed skull.

▲ CRITICAL STEP All surgical tools must be sterile.

6| Using a scalpel, detach the cervical trapezius muscle from the skull, and move it posterior to its attached location, so as to fully expose the skull above the cerebellum (Fig. 1a).

! CAUTION Bleeding will occur during this step.

? TROUBLESHOOTING

7| At this point, all further procedures should be performed under the stereomicroscope. Using a pen, draw a 6-mm circle over the parietal and occipital regions of the skull.

8| Use a high-speed bone microdrill with a 1.4-mm-diameter burr tip to make a groove around the margins of the circle (Fig. 1b).

▲ CRITICAL STEP Drill slowly and apply cold saline regularly to avoid thermally induced injury to the brain.

▲ CRITICAL STEP The bone overlying the cerebellum is thin. Drill slowly and carefully to avoid damage.

? TROUBLESHOOTING

9| Deepen the groove gradually by repetitive drilling, until the bone flap becomes loose and/or the cerebellar surface vessels become visible.

▲ CRITICAL STEP Do not apply excessive pressure. Check the depth of the groove and the thickness of the skull. Some bleeding from the skull may occur.

? TROUBLESHOOTING

10| Use a no. 3 Dumont forceps with great caution to separate the bone flap from the dura mater underneath (Fig. 1c).

▲ CRITICAL STEP Use sterile saline when removing the bone flap. Be careful not to damage the cerebellar surface vasculature.

11| Remove the bone flap very slowly (Fig. 1d).

▲ CRITICAL STEP The dura is attached to the cranium. Dura capillaries may tear, resulting in bleeding. Use Gelfoam and sterile saline to stop the bleeding.

? TROUBLESHOOTING

12| Place a piece of Gelfoam that has been soaked in saline on the dura mater, and rinse it continuously with sterile saline to keep the cerebellum moist.

13| Use a Dumont no. 3 forceps to remove small pieces of bone attached to the edge of the circle.

14| Place Gelfoam on the edge of the cut to absorb saline and/or blood.

15| Use a Dumont no. 5 forceps to make a small opening in the dura mater near the edge.

▲ CRITICAL STEP Do not make the opening close to large cerebellar vessels.

16| Insert the Vannas spring scissors into the opening and cut the dura and the arachnoid membranes from the surface of the cerebellum completely, avoiding damage to large vessels when possible.

▲ **CRITICAL STEP** Start removing the dura from the periphery very slowly. Avoid pulling the dura or putting pressure on the surface of the cerebellum. Bleeding may occur during this step; use Gelfoam and sterile saline to stop the bleeding.

? TROUBLESHOOTING

17| Rinse the surface of the cerebellum with sterile saline.

18| Place a 7-mm-diameter round coverslip (glass or polyethylene) to cover the surface of the exposed cerebellum (Fig. 1e). Use saline to keep the surface wet during this procedure (Fig. 1f). The skull bone should remain dry around the opening.

▲ **CRITICAL STEP** The coverslip should remain as close to the surface as possible.

▲ **CRITICAL STEP** The choice of the coverslip (glass or polyethylene) depends on the imaging application. For multiphoton microscopy, a glass coverslip is preferred, as polyethylene may be burned rapidly by the laser, leading to impairment of the image quality. For ultrasound imaging, a polyethylene coverslip is required because it causes less reflection and enables superior image quality.

19| Fix the coverslip to the bone with a 1:1 mixture of a histocompatible cyanoacrylate glue and fine acrylic powder (Fig. 1g,h). Apply the mixture before it sets.

▲ **CRITICAL STEP** The skull bone should be dried with a dry cotton swab before applying the glue. If the bone is wet, the coverslip can become loose. Be careful to avoid allowing the glue to contact the surface of the cerebellum. Saline should be applied on the exposed surface of the cerebellum to the edge of the coverslip; this will exclude any glue that may escape the demarcated boundary.

? TROUBLESHOOTING

20| Monitor the mouse post surgery, and allow it to rest on the heating pad until it awakens.

21| Once the mouse is awake, place it in its cage, one mouse per cage.

▲ **CRITICAL STEP** If you put more than one mouse in a cage, they may damage the coverslips of their cage mates, leading to potential cerebellar injuries.

▲ **CRITICAL STEP** The next day, administer buprenorphine s.c. at a concentration of 0.1 mg/kg body weight, as needed.

? TROUBLESHOOTING

Implantation of tumor cells (7–10 d post surgery) ● TIMING 20–25 min

▲ **CRITICAL** Steps 22–48 must be carried out only if implanting tumor cells.

22| Administer buprenorphine at a concentration of 0.1 mg/kg body weight 15 min before surgery. Anesthetize the mouse with the ketamine and xylazine mixture (90 and 9 mg/kg body weight, respectively).

23| Apply an ophthalmic lubricant to the eyes.

24| Place the mouse in the stereotactic frame under the bright-field stereomicroscope, and ensure that the head is stabilized.

▲ **CRITICAL STEP** Ensure that the position of the mouse is secure.

25| Use forceps to carefully remove the cerebellar window. Remove the coverslip and glue with a Dumont no. 3 forceps.

▲ **CRITICAL STEP** Remove the cerebellar window very carefully to avoid damage to the coverslip and injuries to the cerebellum. If the window is more than 2 weeks old, it may be necessary to use a 30-gauge needle to gently break the interface between the glue and the coverslip, leaving the glue ring intact on the bone in order to remove only the coverslip.

26| Note the presence of bony regrowth from the skull that may obscure the imaging window. If such a regrowth is present, remove it delicately with fine forceps.

27| Use a dry cotton swab and forceps to clean the bone around the window area.

28| Rinse the cerebellum continuously with sterile saline.

29| Place Gelfoam to absorb the saline and/or blood.

30| Place a Hamilton syringe with the 28-gauge needle filled with medulloblastoma cells (~10,000/μl) on the stereotactic injection device at an angle of 0–10 degrees from perpendicular to the work surface (0–10 degrees offset from the vertical plane).

31| Make sure that the head of the mouse is fixed in the stereotactic device such that the surface of the cerebellum is parallel to the horizontal plane.

32| Remove the Gelfoam.

33| Use the 3D coordination setup of the stereotactic device to place the top of the needle 2 mm posterior to the confluence of the sagittal and transverse sinuses. (See Supplementary Fig. 1a for tumor implantation coordinate map.)

34| Move the needle 2.0–2.5 mm lateral from the confluence of sinuses.

35| Move the needle 2.0–2.5 mm dorsal from its previous position.

36| Carefully lower the needle until it touches, but does not puncture, the surface of the cerebellar hemisphere.

37| Lower the needle ~1 mm into the cerebellum.

▲ **CRITICAL STEP** Surface capillaries may tear, resulting in bleeding. Use Gelfoam and sterile saline to stop the bleeding.

38| Retract the needle ~0.5 mm.

39| Inject 1 µl of cell suspension over 2 min.

40| Rinse the surface of the cerebellum with sterile saline.

41| Retract the needle over 3–5 min, until it exits the cerebellum, rinsing the surface of the cerebellum continuously with sterile saline.

▲ **CRITICAL STEP** The slow retraction coupled with debridement mitigates the migration of tumor cells to the surface of the tissue.

42| Place Gelfoam on the cerebellum to absorb saline and/or blood.

43| Remove the Gelfoam.

44| Rinse the cerebellum with sterile saline.

45| Place a new 7-mm-diameter round coverslip (glass or polyethylene).

46| Fix the coverslip to the bone or to the glue ring with a cyanoacrylate glue/acrylic powder mixture. Add saline to the surface of the cerebellum to the edge of the coverslip to exclude the glue from the cerebellar surface.

47| Place one mouse in a cage.

▲ **CRITICAL STEP** If you put more than one mouse in a single cage, they may damage the coverslips of their cage mates' windows, leading to potential cerebellar injuries.

48| The next day, subcutaneously administer buprenorphine to the mouse at a concentration of 0.1 mg/kg body weight, as needed.

Replacement of window (if needed) ● TIMING 5–15 min

49| The window should remain clear for months. If imaging modality or quality warrants, replace the window as described in Steps 22–29 and 43–48 above.

? TROUBLESHOOTING

? TROUBLESHOOTING—Troubleshooting advice can be found in Table 1.

● TIMING

Steps 1–21, surgery: 45 min

Steps 22–48, implantation of tumor cells (7–10 d post surgery): 20–25 min

Step 49, replacement of window (if needed): 5–15 min

ANTICIPATED RESULTS

After the establishment of the cerebellar window and after the mouse has recovered from anesthesia, simple visual inspection of the cerebellar window should be performed in order to assess its quality. This can be done within the first 2–3 d post surgery. If hemorrhage or other surgery-related complications have interfered with the optical quality of the window, it will be apparent during this time. As mentioned previously, although we have not observed

reactive gliosis in the cerebellum after surgery, we cannot formally exclude it as a possible postsurgical complication; we generally wait at least 7 d before proceeding to further imaging or tumor implantation.

After tumor implantation, imaging of lesions is generally not feasible until 1–2 weeks after implantation, depending on the aggressiveness of the implanted cells and the number of cells injected, as the implanted tumor cells will not have formed a discernible mass until this time. Imaging is possible for all but the end stages of disease, when the mice become moribund and the window quality is compromised.

The surgical preparations described in this protocol allow a spontaneous or implanted tumor to develop and grow in an optically accessible environment of the mouse cerebellum. Longitudinal imaging studies are facilitated, as the cerebellar window could last for several months. Such studies include the longitudinal monitoring of tumor growth using the time- and cost-effective method of ultrasonography, as well as high-resolution multiphoton microscopy and OFDI-based imaging of the tumor pathophysiology. Of note, the cerebellar window described in this protocol may find application not only for pediatric medulloblastoma tumors but also for further primary or secondary malignancies of the cerebellum.

Supplementary Material

Refer to Web version on PubMed Central for supplementary material.

Acknowledgments

References

1. Drew PJ, et al. Chronic optical access through a polished and reinforced thinned skull. Nat Methods. 2010; 7:981–984. [PubMed: 20966916]

2. Grutzendler J, Kasthuri N, Gan WB. Long-term dendritic spine stability in the adult cortex. Nature. 2002; 420:812–816. [PubMed: 12490949]

3. Chow DK, et al. Laminar and compartmental regulation of dendritic growth in mature cortex. Nat Neurosci. 2009; 12:116–118. [PubMed: 19151711]

4. Brown EB, et al. In vivo measurement of gene expression, angiogenesis and physiological function in tumors using multiphoton laser scanning microscopy. Nat Med. 2001; 7:864–868. [PubMed: 11433354]

5. Cabrales, P., Carvalho, LJ. Intravital microscopy of the mouse brain microcirculation using a closed cranial window; J Visual Exp. 2010. p. e2184http://dx.doi.org/10.3791/2184

6. Holtmaat A, et al. Long-term, high-resolution imaging in the mouse neocortex through a chronic cranial window. Nat Protoc. 2009; 4:1128–1144. [PubMed: 19617885]

7. Goldey GJ, et al. Removable cranial windows for long-term imaging in awake mice. Nat Protoc. 2014; 9:2515–2538. [PubMed: 25275789]

8. Snuderl M, et al. Targeting placental growth factor/neuropilin 1 pathway inhibits growth and spread of medulloblastoma. Cell. 2013; 152:1065–1076. [PubMed: 23452854]

9. Yuan F, et al. Vascular permeability and microcirculation of gliomas and mammary carcinomas transplanted in rat and mouse cranial windows. Cancer Res. 1994; 54:4564–4568. [PubMed: 8062241]

10. Foersch S, et al. Confocal laser endomicroscopy for diagnosis and histomorphologic imaging of brain tumors *in vivo*. PLoS One. 2012; 7:e41760. [PubMed: 22911853]

11. Vakoc BJ, et al. Three-dimensional microscopy of the tumor microenvironment *in vivo* using optical frequency domain imaging. Nat Med. 2009; 15:1219–1223. [PubMed: 19749772]

12. Kodack DP, et al. Combined targeting of HER2 and VEGFR2 for effective treatment of HER2-amplified breast cancer brain metastases. Proc Natl Acad Sci USA. 2012; 109:E3119–E3127. [PubMed: 23071298]

13. Askoxylakis V, et al. Preclinical efficacy of Ado-trastuzumab emtansine in the brain microenvironment. J Natl Cancer Inst. 2016; 108 http://dx.doi.org/10.1093/jnci/djv313.

14. Lathia JD, et al. Direct *in vivo* evidence for tumor propagation by glioblastoma cancer stem cells. PLoS One. 2011; 6:e24807. [PubMed: 21961046]

15. Strachan CJ, Windbergs M, Offerhaus HL. Pharmaceutical applications of non-linear imaging. Int J Pharm. 2011; 417:163–172. [PubMed: 21182913]

16. Yun S, Tearney G, de Boer J, Iftimia N, Bouma B. High-speed optical frequency-domain imaging. Opt Exp. 2003; 11:2953–2963.

17. Tannous BA. Gaussia luciferase reporter assay for monitoring biological processes in culture and *in vivo*. Nat Protoc. 2009; 4:582–591. [PubMed: 19373229]

18. Bovenberg MS, Degeling MH, Tannous BA. Enhanced *Gaussia* luciferase blood assay for monitoring of *in vivo* biological processes. Anal Chem. 2012; 84:1189–1192. [PubMed: 22148161]

19. Prajapati SI, et al. MicroCT-based virtual histology evaluation of preclinical medulloblastoma. Mol Imaging Biol. 2011; 13:493–499. [PubMed: 20617390]

20. Suero-Abreu GA, et al. In vivo Mn-enhanced MRI for early tumor detection and growth rate analysis in a mouse medulloblastoma model. Neoplasia. 2014; 16:993–1006. [PubMed: 25499213]

21. Samano AK, et al. Functional evaluation of therapeutic response for a mouse model of medulloblastoma. Transg Res. 2010; 19:829–840.

22. Nelson AL, et al. Magnetic resonance imaging of patched heterozygous and xenografted mouse brain tumors. J Neuro-Oncol. 2003; 62:259–267.

23. Jain, RK., et al. Intravital microscopy of normal and diseased tissues in the mouse in Live Cell Imaging: A Laboratory Manual. Cold Spring Harbor Laboratory Press; Cold Spring Harbor, New York: 2005. p. 435-466.

24. Vakoc BJ, Fukumura D, Jain RK, Bouma BE. Cancer imaging by optical coherence tomography: preclinical progress and clinical potential. Nat Rev Cancer. 2012; 12:363–368. [PubMed: 22475930]

25. Niermann KJ, et al. Measuring tumor perfusion in control and treated murine tumors: correlation of microbubble contrast-enhanced sonography to dynamic contrast-enhanced magnetic resonance imaging and fluorodeoxyglucose positron emission tomography. J Ultrasound Med. 2007; 26:749–756. [PubMed: 17526606]

26. Kamoun WS, et al. Simultaneous measurement of RBC velocity, flux, hematocrit and shear rate in vascular networks. Nat Methods. 2010; 7:655–660. [PubMed: 20581828]

27. Fukumura D, Duda DG, Munn LL, Jain RK. Tumor microvasculature and microenvironment: novel insights through intravital imaging in pre-clinical models. Microcirculation. 2010; 17:206–225. [PubMed: 20374484]

28. Jain RK, Munn LL, Fukumura D. Dissecting tumour pathophysiology using intravital microscopy. Nat Rev Cancer. 2002; 2:266–276. [PubMed: 12001988]

29. Kloepper J, et al. Ang-2/VEGF bispecific antibody reprograms macrophages and resident microglia to anti-tumor phenotype and prolongs glioblastoma survival. Proc Natl Acad Sci USA. 2016; 113:4476–4481. [PubMed: 27044098]

30. Gillies RJ, Anderson AR, Gatenby RA, Morse DL. The biology underlying molecular imaging in oncology: from genome to anatome and back again. Clin Radiol. 2010; 65:517–521. [PubMed: 20541651]

31. Folarin AA, Konerding MA, Timonen J, Nagl S, Pedley RB. Three-dimensional analysis of tumour vascular corrosion casts using stereoimaging and micro-computed tomography. Microvasc Res. 2010; 80:89–98. [PubMed: 20303995]

32. Lassau N, et al. Metastatic renal cell carcinoma treated with sunitinib: early evaluation of treatment response using dynamic contrast-enhanced ultrasonography. Clin Cancer Res. 2010; 16:1216–1225. [PubMed: 20145174]

33. Walk EL, McLaughlin S, Coad J, Weed SA. Use of high frequency ultrasound to monitor cervical lymph node alterations in mice. PLoS One. 2014; 9:e100185. [PubMed: 24955984]

34. Horie S, Chen R, Li L, Mori S, Kodama T. Contrast-enhanced high-frequency ultrasound imaging of early stage liver metastasis in a preclinical mouse model. Cancer Lett. 2013; 339:208–213. [PubMed: 23791880]

35. Sastra SA, Olive KP. Quantification of murine pancreatic tumors by high-resolution ultrasound. Methods Mol Biol. 2013; 980:249–266. [PubMed: 23359158]

36. Li L, et al. Enhanced sonographic imaging to diagnose lymph node metastasis: importance of blood vessel volume and density. Cancer Res. 2013; 73:2082–2092. [PubMed: 23333937]

37. Xuan JW, et al. Functional neoangiogenesis imaging of genetically engineered mouse prostate cancer using three-dimensional power Doppler ultrasound. Cancer Res. 2007; 67:2830–2839. [PubMed: 17363606]

38. Weigert R, Porat-Shliom N, Amornphimoltham P. Imaging cell biology in live animals: ready for prime time. J Cell Biol. 2013; 201:969–979. [PubMed: 23798727]

39. Alexander S, Weigelin B, Winkler F, Friedl P. Preclinical intravital microscopy of the tumour-stroma interface: invasion, metastasis, and therapy response. Curr Opin Cell Biol. 2013; 25:659–671. [PubMed: 23896198]

40. Jain RK. Antiangiogenesis strategies revisited: from starving tumors to alleviating hypoxia. Cancer Cell. 2014; 26:605–622. [PubMed: 25517747]

41. Helmlinger G, Yuan F, Dellian M, Jain RK. Interstitial pH and pO2 gradients in solid tumors *in vivo*: high-resolution measurements reveal a lack of correlation. Nat Med. 1997; 3:177–182. [PubMed: 9018236]

42. Kashiwagi S, et al. Perivascular nitric oxide gradients normalize tumor vasculature. Nat Med. 2008; 14:255–257. [PubMed: 18278052]

43. Martin GR, Jain RK. Noninvasive measurement of interstitial pH profiles in normal and neoplastic tissue using fluorescence ratio imaging microscopy. Cancer Res. 1994; 54:5670–5674. [PubMed: 7923215]

44. Chauhan VP, et al. Normalization of tumour blood vessels improves the delivery of nanomedicines in a size-dependent manner. Nat Nanotechnol. 2012; 7:383–388. [PubMed: 22484912]

45. Ager EI, et al. Blockade of MMP14 activity in murine breast carcinomas: implications for macrophages, vessels, and radiotherapy. J Natl Cancer Inst. 2015; 107:djv017. [PubMed: 25710962]

46. Goel S, et al. Effects of vascular-endothelial protein tyrosine phosphatase inhibition on breast cancer vasculature and metastatic progression. J Natl Cancer Inst. 2013; 105:1188–1201. [PubMed: 23899555]

47. Kirkpatrick ND, et al. Video-rate resonant scanning multiphoton microscopy: an emerging technique for intravital imaging of the tumor microenvironment. Intravital. 2012; 1:60–68.

48. Li W, et al. Intravital 2-photon imaging of leukocyte trafficking in beating heart. J Clin Invest. 2012; 122:2499–2508. [PubMed: 22706307]

49. Bajenoff M, et al. Stromal cell networks regulate lymphocyte entry, migration, and territoriality in lymph nodes. Immunity. 2006; 25:989–1001. [PubMed: 17112751]

50. Egeblad M, et al. Visualizing stromal cell dynamics in different tumor microenvironments by spinning disk confocal microscopy. Dis Models Mech. 2008; 1:155–167. discussion 165.

51. Sasaki A, Melder RJ, Whiteside TL, Herbermann RB, Jain RK. Preferential localization of human adherent lymphokine-activated killer cells in tumor microcirculation. J Natl Cancer Inst. 1991; 83:433–437. [PubMed: 1999850]

52. Perentes JY, et al. In vivo imaging of extracellular matrix remodeling by tumor-associated fibroblasts. Nat Methods. 2009; 6:143–145. [PubMed: 19151720]

53. Chauhan VP, et al. Angiotensin inhibition enhances drug delivery and potentiates chemotherapy by decompressing tumour blood vessels. Nat Commun. 2013; 4:2516. [PubMed: 24084631]

54. Wei SC, et al. Matrix stiffness drives epithelial-mesenchymal transition and tumour metastasis through a TWIST1-G3BP2 mechanotransduction pathway. Nat Cell Biol. 2015; 17:678–688. [PubMed: 25893917]

55. Nakasone ES, et al. Imaging tumor-stroma interactions during chemotherapy reveals contributions of the microenvironment to resistance. Cancer Cell. 2012; 21:488–503. [PubMed: 22516258]

56. Condeelis J, Segall JE. Intravital imaging of cell movement in tumours. Nat Rev Cancer. 2003; 3:921–930. [PubMed: 14737122]

57. Kedrin D, et al. Intravital imaging of metastatic behavior through a mammary imaging window. Nat Methods. 2008; 5:1019–1021. [PubMed: 18997781]

58. Wyckoff JB, et al. Direct visualization of macrophage-assisted tumor cell intravasation in mammary tumors. Cancer Res. 2007; 67:2649–2656. [PubMed: 17363585]

59. Vuong B, et al. Measuring the optical characteristics of medulloblastoma with optical coherence tomography. Biomed Opt Exp. 2015; 6:1487–1501.
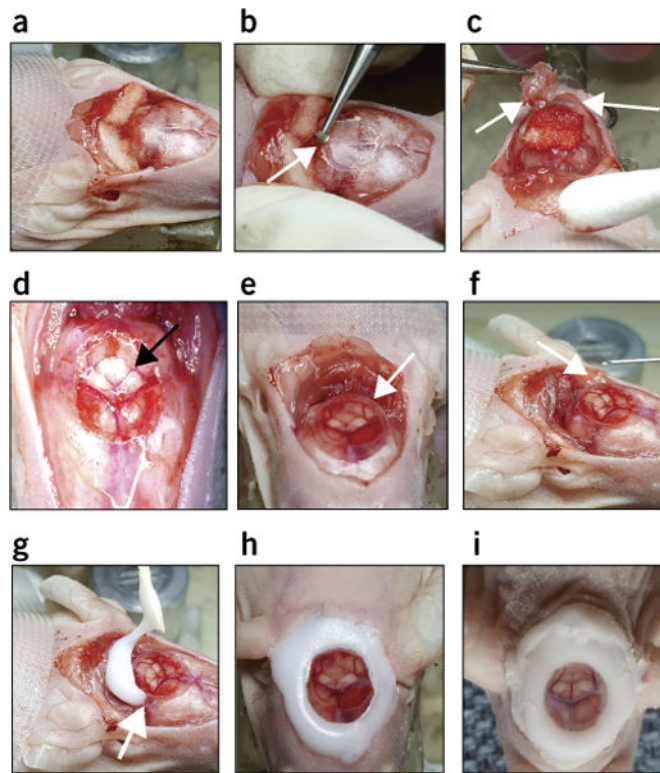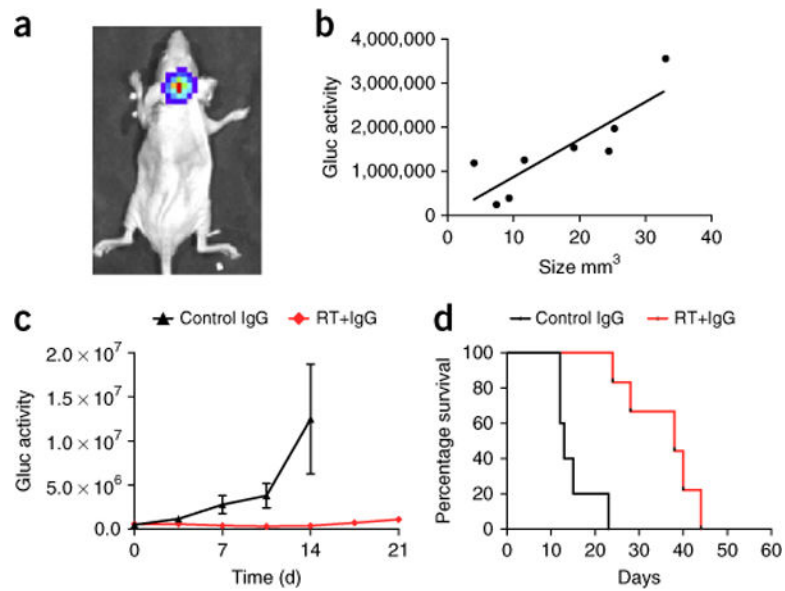
Figure 1.

Procedure for implantation of a cerebellar window. (**a**) Remove skin flap, push back the upper neck muscles, and add Gelfoam. (**b**) Gently drill bone to expose the top of the cerebellum (arrow points to the drill on the surface of the skull). (**c**) Remove skull piece and keep it moist with Gelfoam (arrows point to the removed skull piece). (**d**) View of the exposed cerebellum through a light microscope (arrow points to the exposed cerebellum). (**e**) Place the coverslip (glass or polyethylene) to cover the opening (arrow points to the coverslip). (**f**) Add saline drops under the coverslip to avoid air bubbles (arrow points to the site of injection under the coverslip). (**g**) Apply glue at the coverslip–skull bone junction (arrow points to the glue at the coverslip–skull bone junction).
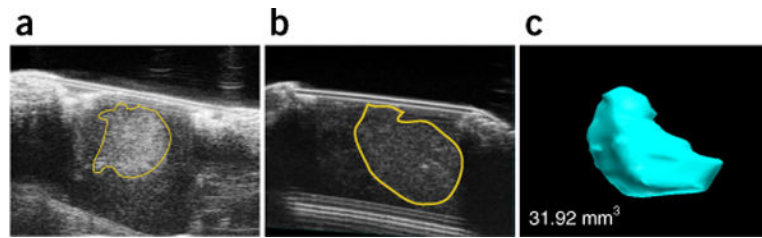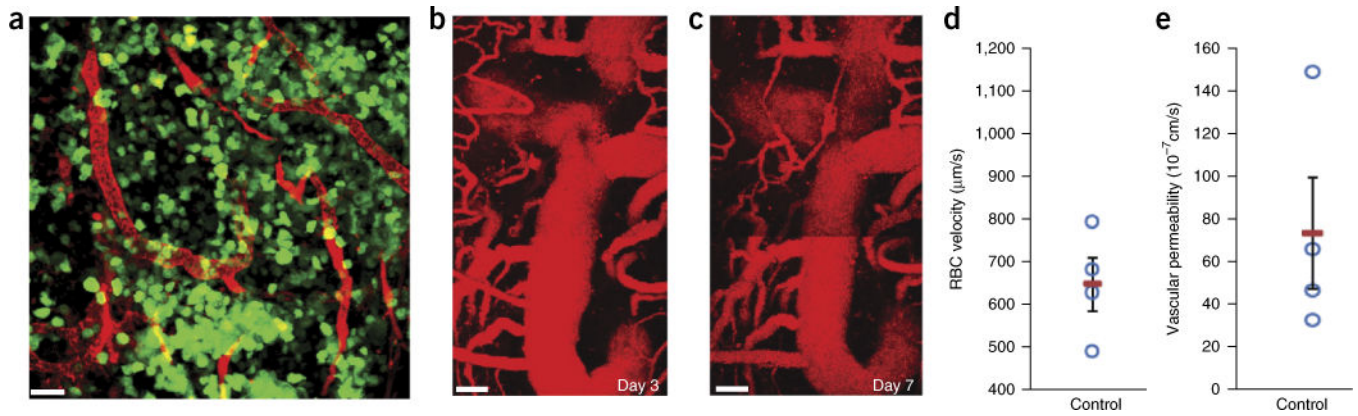
Figure 2.
Ultrasonography-based imaging through the cerebellar window. (**a**) Ultrasonography imaging through a cerebellar window of a human medulloblastoma tumor (D283-MED) stereotactically implanted into the cerebellum of a nude mouse. (**b**) Ultrasonography imaging of a spontaneous medulloblastoma in a Smo/Smo mouse. (**c**) Corresponding 3D reconstruction of the tumor from **b**. Imaging and tumor-volume assessment were performed through a cerebellar window using a polyethylene coverslip and a Vevo 2100 high-frequency ultrasonography device (FujiFilm VisualSonics). All animal procedures were performed according to the guidelines of the Public Health Service Policy on Human Care of Laboratory Animals and in accordance with a protocol approved by the Institutional Animal Care and Use Committee of Massachusetts General Hospital. All cell lines used in the experiments depicted were tested both for authenticity (by short tandem-repeat typing) and for mycoplasma contamination, and certified to be both authentic medulloblastoma cell lines and mycoplasma free.
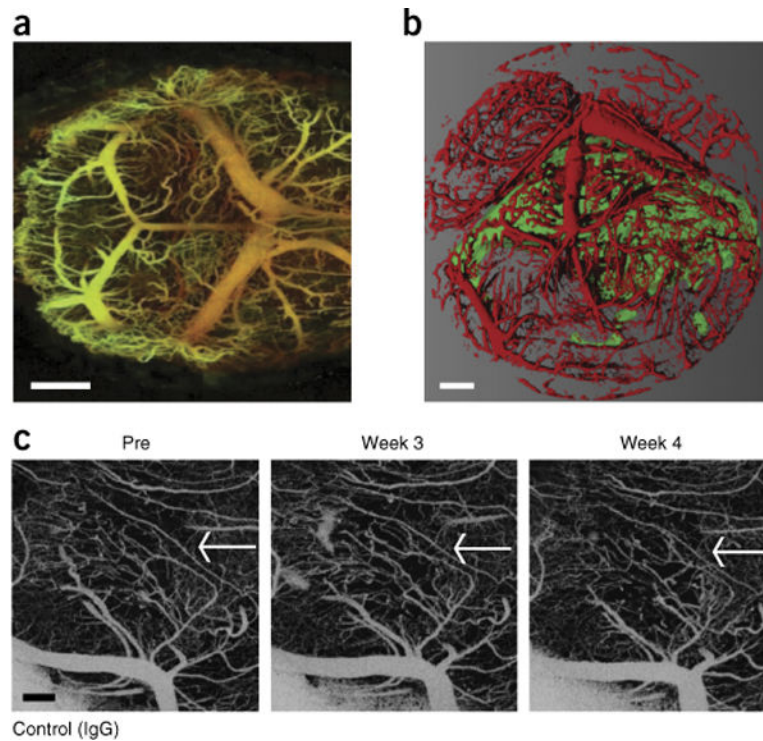
Figure 3.
Cerebellar windows can be applied for the evaluation of indirect surrogates of tumor growth and response to therapies. (**a**) Bioluminescence image of a human medulloblastoma xenograft (D283-MED-Gluc) stereotactically implanted into the cerebellum of a nude mouse. Imaging was performed after retro-orbital injection of a coelenterazine solution (4 mg/kg body weight) using an *in vivo* imaging system (IVIS Lumina II; Caliper Life Sciences). (**b**) Correlation between blood Gluc activity and tumor volume for D283-MED-Gluc medulloblastomas growing in the mouse cerebellum, as measured by ultrasonography-based imaging using a cerebellar window ($n = 8$). (**c**) Nude mice with medulloblastoma D283-MED-Gluc tumors in the cerebellum were treated with a nonspecific antibody alone or in combination with radiation therapy (2×1.8 Gy), and blood Gluc activity was measured over time, as previously described ($n = 5$–6 per group)[12]. Gluc activity was measured as relative light units per s. (**d**) Survival analysis of mice from **c**. The survival end point was reached when mice lost > 20% of their body weight or exhibited signs of prolonged distress or neurological impairment. All animal procedures were performed according to the guidelines of the Public Health Service Policy on Human Care of Laboratory Animals and in accordance with a protocol approved by the Institutional Animal Care and Use Committee of Massachusetts General Hospital. All cell lines used in the experiments depicted were tested both for authenticity (by short tandem-repeat typing) and for mycoplasma contamination and were certified to be both authentic medulloblastoma cell lines and mycoplasma free. RT, radiation therapy.

Figure 4.
Intravital multiphoton microscopy imaging of D283-MED-Gluc medulloblastomas in the cerebellum of mice using a cerebellar window. (**a**) Intravital multiphoton microscopy images illustrate the medulloblastoma cells (green) in the cerebellum and the tumor vasculature (red). Tumor cells expressing GFP (green) and blood vessels (red) are contrast-enhanced by i.v. injection of tetramethylrhodamine dextran (2,000,000 molecular weight; scale bar, 50 μm). (**b**) D283-MED-Gluc vessels imaged after i.v. injection of tetramethylrhodamine–BSA (68,000 molecular weight; scale bar, 50 μm) fluorescently labeled red blood cells (RBCs). (**c**) For quantification of vascular function, fluorescently labeled red blood cells (1,1′-dioctadecyl-3,3′,3′-tetramethylindodicarbocyanine (DiD)) were line-scanned (scale bar, 50 μm). (**d**) The velocity of RBCs was measured by photometric detection of the time required for RBCs to pass between two predetermined positions. (**e**) Vascular permeability was assessed by quantifying the leakage of tetramethylrhodamine–BSA from the vascular to the extravascular space over a 45-min period. All animal procedures were performed according to the guidelines of the Public Health Service Policy on Human Care of Laboratory Animals and in accordance with a protocol approved by the Institutional Animal Care and Use Committee of Massachusetts General Hospital. All cell lines used in the experiments depicted were tested both for authenticity (by short tandem-repeat typing) and for mycoplasma contamination and certified to be both authentic medulloblastoma cell lines and mycoplasma free.

Figure 5.
OFDI through a cerebellar window. (**a**) Normal mouse cerebellum (scale bar, 500 μm). (**b**) Medulloblastoma (green)—recognized by the combination of the contrast in 'structure' and 'angiography' parameters—and the vascular network (red)—recognized by the 'angiography' OFDI signal—in the mouse cerebellum (scale bar, 500 μm). (**c**) Serial imaging of the vasculature of medulloblastoma through a cerebellar window. The white arrows indicate the tumor area (scale bar, 100 μm). All animal procedures were performed according to the guidelines of the Public Health Service Policy on Human Care of Laboratory Animals and in accordance with a protocol approved by the Institutional Animal Care and Use Committee of Massachusetts General Hospital. All cell lines used in the experiments depicted were tested both for authenticity (by short tandem-repeat typing) and for mycoplasma contamination and certified to be both authentic medulloblastoma cell lines and mycoplasma free.

TABLE 1

Troubleshooting table.

Step	Problem	Possible reason	Solution(s)
6, 8, 9, 11, 16	Bleeding from the skull	Injury to blood vessel	Soak up blood with Gelfoam and rinse with sterile saline
8	Drill breaches the skull and the underlying tissue	Speed or force applied was too great	Exclude the mouse from the study; in future surgeries, drill slowly and carefully
Any	Brain swelling	Edema and trauma to the brain; insufficient anesthesia	Administer additional anesthesia (in 50-μl increments until pedal reflex is negative, for a 25-g mouse)
19	Air bubble present in saline	Saline was dispensed too rapidly or an air bubble was present in the syringe	Manipulate or aspirate the saline to remove the bubble
	Glue contacts brain	Saline was not dispensed properly or in sufficient quantity to repel the glue	Dispense an adequate amount of saline, carefully apply the glue
21 and beyond	Regrowth of bone over the cerebellum	Insufficient removal of bone during initial surgery	Before implantation of cells (second surgery), remove the bony regrowth
	Cerebellar window becomes loose or dislodged	Window was manipulated by cage mates	Ensure that mice are housed singly
	Coverslip breaks or becomes otherwise unsuitable for imaging	Excessive force was applied to the coverslip during surgical or imaging procedures	Be gentle when contacting the coverslip; exchange the coverslip for a new one (if before implantation of cells, the coverslip can be exchanged during the second surgery)
	Bleeding occurs after the cerebellar window has been established	Dura and/or blood vessels have been compromised	If bleeding continues, exclude the mouse from the study, as imaging will generally be suboptimal
Post-procedure imaging	Excessive motion (in terms of amplitude and/or frequency) during imaging	The mouse is incompletely anesthetized or the head is insufficiently stabilized	Ensure that anesthesia is sufficient to continue imaging; some motion is normal, but adequately stabilizing the head should allow for acquisition of high-quality images
	Tumor burden is not detectable by ultrasonography	Tumors may be too small or have insufficient contrast to image; there may be multiple small lesions instead of a single large lesion	Use Gluc values to detect implanted tumors, as this method is extremely sensitive; if ultrasound is required, wait until tumors reach threshold size for detection